Available online at www.sciencedirect.com
SCIENCE DIRECT
Polymer 46 (2005) 12430–12439
polymer
www.elsevier.com/locate/polymer

Poly(butylene sucinate-*co*-adipate)/montmorillonite nanocomposites: effect of organic modifier miscibility on structure, properties, and viscoelasticity

Suprakas Sinha Ray, Mosto Bousmina *

Department of Chemical Engineering, Laval University (CREPEC), Que., Canada G1K 7P4

Received 3 August 2005; received in revised form 18 October 2005; accepted 24 October 2005

Abstract

Poly(butylene succinate-*co*-adipate) (PBSA)/layered silicate nanocomposites were prepared by melt extrusion of PBSA and three different types of commercially available organically modified montmorillonite (OMMT). Using three types of OMMT modified with three different kinds of surfactants, the effect of organic modification on nanocomposites was investigated by focusing of three major aspects: morphological study, property measurements, and melt rheological behavior under both small and large deformation flows. X-ray diffraction (XRD) patterns revealed that increasing the level of interactions (miscibility) between the organic modifier and PBSA matrix increases the tendency of the silicate layers to delaminate and distributed nicely within the PBSA matrix. Transmission electron micrographic (TEM) observations showed that the ordering of silicate layers in PBSA matrix is well matched with the XRD patterns. Thermal analysis revealed that extent of crystallinity of PBSA matrix is directly related to the extent of exfoliation of silicate layers in the nanocomposites. Dynamic mechanical analysis and tensile property measurements showed concurrent improvement in mechanical properties when compared to the neat PBSA and the extent of improvement is directly related to the extent of delamination of silicate layers in the PBSA matrix. The same tendency was also observed in melt rheological measurements.

Keywords: Poly(butylene succinate-*co*-adipate); Nanocomposites; Properties

1. Introduction

Poly(butylene succinate-*co*-adipate) (PBSA) is an environmental benign biodegradable polymer made of butylene succinate adipate random copolymer [1,2]. It is synthesized by polycondensation of 1,4-butanediol with succinic and adipic acids [3,4]. A schematic view of the chemical structure of the pure PBSA is illustrated in Fig. 1. PBSA is thermoplastic polyester with many interesting properties, including biodegradability; melt processability and chemical resistance. Because of the 'green' feature, it has been proposed as a degradable plastic for uses in service-ware, grocery, waste-composting bags, mulch films, etc [5]. However, its poor properties such as softness, gas-barrier, and thermal stability limit its end-use applications.

Confinement of polymer chains in a two dimensional silicate gallery, so-called polymer/layered silicate (PLS) nanocomposite, is one of the effective ways to improve the performances of neat polymer concurrently [6–11]. Pristine layered silicates usually contain hydrated Na^+ or K^+ ions [12] and can interact with hydrophilic polymers, such as poly(ethylene oxide) (PEO), [13] or poly(vinyl alcohol) (PVA) [14]. To ensure interfacial interactions of the layered silicates with other polymer matrices, one must convert the normally hydrophilic silicate surface to an organophilic one, making the intercalation of many engineering polymers possible. Generally, this can be achieved by ion-exchange reactions with cationic surfactants including primary, secondary, tertiary, and quaternary alkylammonium or alkylphosphonium cations. Such surfactants lower the surface energy of the inorganic host and improve its wetting with hydrophobic polymer matrices. Additionally, the alkylammonium or alkylphosphonium cations can provide functional groups that can react with the polymer matrix, or in some cases initiate the polymerization of monomers to improve the strength of the interface between the inorganic and the polymer matrix [15,16].

The main objective of this work was to understand the effect of the nature of the surfactant used in clay modification on the

* Corresponding author. Tel.: +1 418 656 2769; fax: +1 418 656 5933.
E-mail address: bousmina@gch.ulaval.ca (M. Bousmina).

0032-3861/$ - see front matter © 2005 Elsevier Ltd. All rights reserved.
doi:10.1016/j.polymer.2005.10.102

$$[-\{O-(CH_2)_4-O\}_1-\{CO-(CH_2)_2-CO-\}_x-\{CO-(CH_2)_4-CO-\}_y-]_n \quad x+y=1$$

Fig. 1. Chemical structure of PBSA.

extent of intercalation of PBSA chains into the silicate galleries. By varying the hydrophobicity, and consequently the favorable interactions of the surfactant with the polymer matrix, a spectrum of structures including phase-separated, intercalated, disordered intercalated, and intercalated-exfoliated can be obtained. Finally, the effects of silicate layers dispersion on various properties such as thermal, mechanical, thermal stability, and melt-rheological properties of nanocomposites were examined.

2. Experimental

2.1. Materials

PBSA used in this study was commercial product from Showa High Polymer Ltd, Japan, with the designation BIONOLLE # 3001, which according to the supplier, has weight average molecular weight, $M_w = 190$ kg/mol. PBSA was dried under vacuum at 50 °C for 36 h prior to use.

Two different types of quaternary and one tertiary ammonium salts, having different chemical structures, were used in this work for the modification of pristine MMT. These organically modified MMTs (OMMTs) were purchased from the Southern Clay Products, Inc. The chemical structure of the specific surfactant and the cation exchange capacity of each of the OMMT are presented in Table 1.

2.2. Nanocomposite preparation

The nanocomposites of PBSA were prepared through melt-extrusion technique using a twin rotor thermohaake-mixer (Polylab system) operated at 135 °C and a rotor speed of 60 rpm for 8 min. Each OMMT was added after two and half minutes of melting of PBSA inside the mixer, which was considered as time zero. For each nanocomposite, the amount of OMMT loading was fixed to 6 wt%. Nanocomposites prepared with three different types of OMMTs were correspondingly abbreviated as PBSA/C15A, PBSA/C93A, and PBSA/C30B for C15A, C93A, and C30B respectively. The obtained nanocomposite strands were then dried under vacuum at 65 °C for 7 h to remove any residual water. The dried nanocomposite samples were then converted into sheets with a thickness of 0.7–2 mm using a Carver laboratory press at 2 MPa at 135 °C for 3 min. The molded samples were cooled at room temperature and then annealed at 60 °C for 5 h to crystallize isothermally before being subjected to mechanical testing.

2.3. Characterization and property measurements

2.3.1. Gel permeation chromatography (GPC)

The molecular weight of PBSA before and after nanocomposites preparation with three different types of OMMTs was determined by means of GPC (Viscotek), using polystyrene standards for calibration and chloroform as a carrier solvent at 40 °C with the flow rate of 0.5 mL/min. GPC data clearly indicate that there is no degradation of PBSA matrix after nanocomposites preparation with three different kinds of OMMT. The thermal stability of PBSA was also verified by

Table 1
Characteristics of organically modified montmorrilonite (OMMT) used in this research

Organoclay Type	Code	Modifier concentration (meq/100 g)	Chemical structure of organic modifier[a]	δ of organic modifier[b,c]
Cloisite 15A	C15A	125	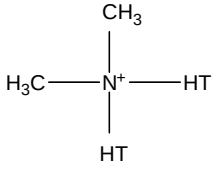	16.94
Cloisite 93A	C93A	90	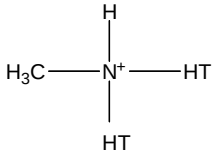	17.96
Cloisite 30B	C30B	90	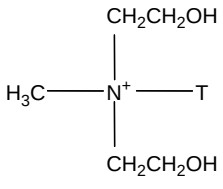	21.5

[a] T is tallow and HT is hydrogenated tallow (~65% C18; ~30% C16; ~5% C14).
[b] δ is the solubility parameter calculated by group contribution method of Fedors.
[c] δ value of neat PBSA is 23.8.

thermogavimetric analyses that didn't reveal any degradation for 4 h at the mixing temperature.

2.3.2. X-ray diffraction (XRD)

XRD experiments were conducted on a Simens-500 diffractometer. The beam was Cu Kα radiation (λ = 0.154 nm) operated at 40 kV and 40 mA. The data were obtained from $2\theta = 1$–25° at a scanning speed of 0.12 °C/min. The basal spacing of clay (pristine or organically modified) before and after intercalation was estimated from the position of (d_{001}) peak in the XRD pattern.

2.3.3. Transmission electron microscopy (TEM)

Dispersability of the intercalated silicate layers in the PBSA matrix was evaluated by means of TEM (JEOL model JEM-1230 instrument) operated at an accelerating voltage of 80 kV. The TEM specimens were about 50–70 nm thick. They were prepared by ultramicrotoming the nanocomposite samples encapsulated in epoxy matrix with a diamond knife.

2.3.4. Differential scanning calorimetry (DSC)

The glass transition temperature (T_g), melting temperature (T_m), and heat of fusion (ΔH_m) of pure PBSA and the three different nanocomposites were measured by using DSC Q100 system (TA Instruments), over a temperature range of −90 to 150 °C at a scan rate of 10 °C/min under nitrogen atmosphere.

2.3.5. Dynamic mechanical analysis (DMA)

Dynamic mechanical properties of neat PBSA and various nanocomposites were measured by using a Rheometrics Scientific Analyzer (RSA) in the dual cantilever bending mode. The temperature dependence of storage flexural modulus (E') of neat PBSA and nanocomposites were measured at a constant frequency (ω) of 6.28 rad/s with the strain amplitude of 0.02% and in the temperature range of −65 to 75 °C with a heating rate of 2 °C/min.

2.3.6. Tensile properties

Test specimens for the tensile property (in the traction mode) measurements were prepared from 1.5-mm-thick plates according to the ASTM D 638. The tensile modulus, tensile yield strength, and elongation at break were measured with a hydraulic tensile Instron 88215 tester (load 5KN) at the strain rate of 5 cm/min at room temperature. The data presented here are averages of eight tests with a maximum error of 9%.

2.3.7. Thermogravimetric analysis (TGA)

The thermogravimetric analyses (TGA) were conducted on a TGA Q500 (TA Instruments) at a heating rate of 10 °C/min under air, from room temperature to 700 °C.

2.3.8. Melt rheology

Melt rheological measurements were performed on Paar-Physica MCR 500 Rheometer in parallel plate geometry using 25 mm diameter parallel plates. All studies were conducted at 120 °C. Linear viscoelastic zone was assessed by performing strain sweep tests both at small and high frequencies. Frequency sweep tests from 0.01 to 100 rad s^{-1} were performed at 5% strain.

Steady-shear viscosity measurements were also conducted at 120 °C using 25 mm diameter cone and plate geometry with a cone angle of 0.1 rad.

3. Results and discussion

3.1. XRD Patterns of organoclays

The distance between the silicate galleries in clay is directly provided by the XRD patterns in the range of $2\theta = 1$ to10°. The XRD patterns of pristine MMT and three different OMMT powders are shown in Fig. 2. The mean interlayer distance of the (001) plane ($d_{(001)}$) for the pristine MMT and three OMMTs are varies in this order: C15A > C93A > C30B > CNa. Therefore, on the basis of above results it may be expected that C15A will be the suitable organoclay for the preparation of nanocomposite with PBSA because it has larger $d_{(001)}$ spacing as compared to that of C93A and C30B, which is presumed to facilate the polymer chains penetration into the confined space between the silicate layers.

3.2. Nanocomposite structure

The nanocomposite structure was characterized by XRD pattern and TEM observations. Direct evidence of the intercalation of the polymer chain into the silicate galleries is provided by XRD patterns in the range of $2\theta = 1$–10°. Fig. 3(a) shows the result of XRD patterns of pure CNa powder and corresponding PBSA/CNa composite prepared with 6 wt% of pristine MMT. The characteristic mean interlayer spacing of the (001) plane ($d_{(001)}$) for the CNa solid is 1.2 nm. In the case of PBSA/CNa hybrid, the intensity of the characteristic peak of CNa in PBSA/CNa is significantly reduced due to the dilution effect, but the angle of diffraction retains at the same position, indicating the formation of conventional composite. Such a

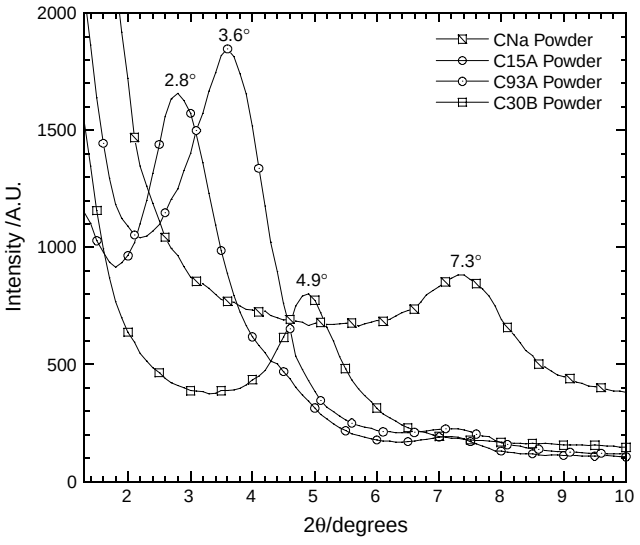

Fig. 2. XRD patterns of pristine and three different organically modified MMT.

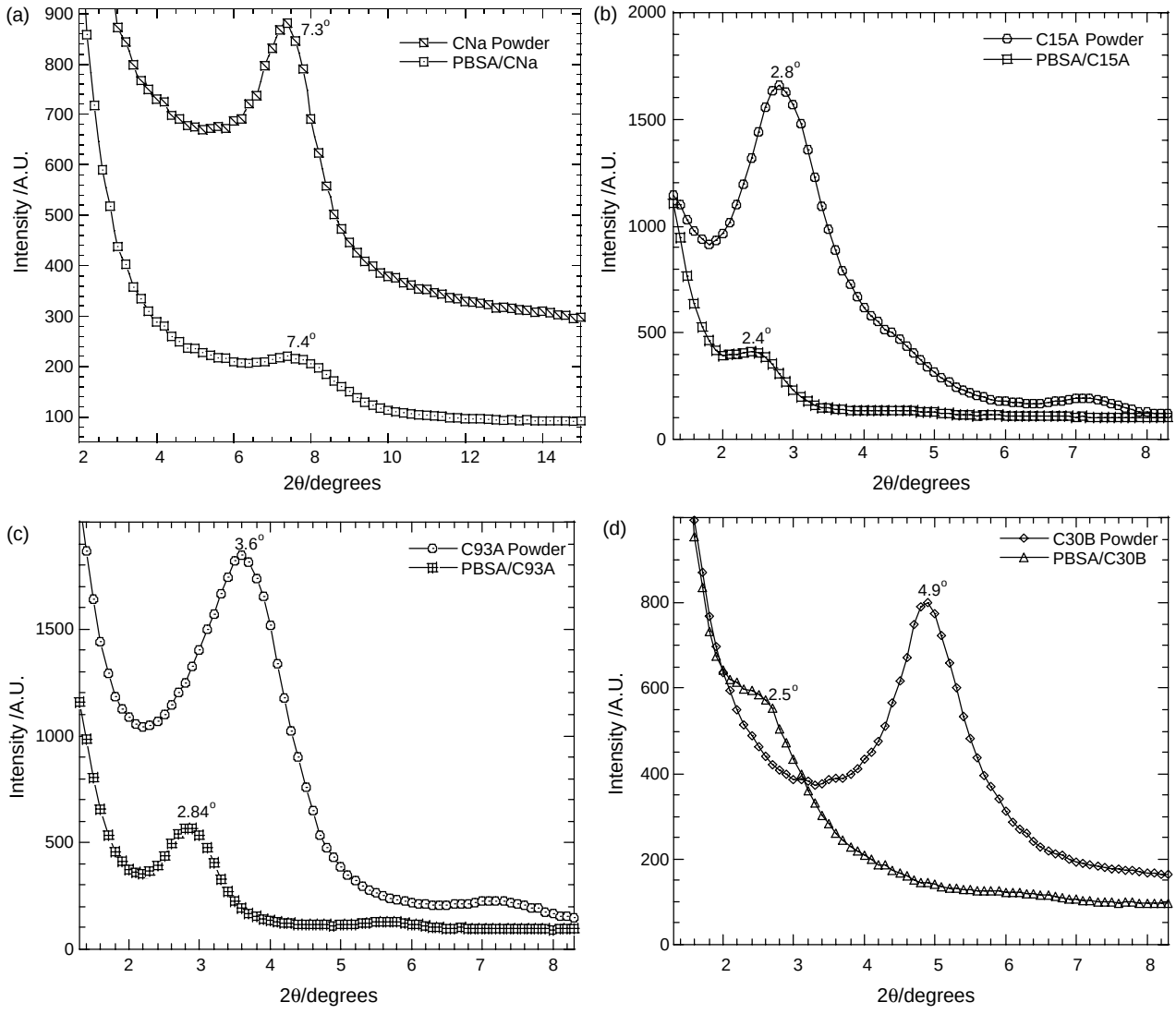

Fig. 3. XRD patterns of (a) CNa and PBSA/CNa hybrid, (b) C15A and PBSA/C15A nanocomposite, (c) C93A and PBSA/C93A nanocomposite, and (d) C30B and PBSA/C30B nanocomposite.

result is natural because PBSA matrix has no favorable interactions with the hydrophilic CNa surface.

The XRD patterns of C15A powder and the corresponding PBSA/C15A hybrid are shown in Fig. 3(b). The characteristic peak of C15A corresponding to the (001) interlayer spacing shifted to the smaller angle due to the intercalation of PBSA chains into the silicate galleries. This corresponds to an interlamellar *d*-spacing of 3.68 nm. For PBSA/C93A such a distance is 3.1 nm (Fig. 3(c)). In the XRD pattern of PBSA/C30B, the intensity of the characteristic peak of C30B is significantly reduced and a small shoulder peak is observed at $2\theta = 2.5^\circ$ ($d_{(001)} = 3.53$ nm), indicating that the structure is potentially highly intercalated, due to the strong interaction between the 'CO' group on the PBSA backbone (see Fig. 1) with the diols present in the C30B.

Such a result seems a priori in contradiction with the initial interlamellar spacing of the modified clays. Recently we have shown that the initial *d*-spacing favors the intercalation process in polymer blends modified with clay [17]. The results have shown that high initial *d*-spacing was favorable for the compatibilization process but not for the exfoliation of the lamellae within the two-phase system. Here also the larger initial *d*-spacing does not guarantee favorable interactions of the matrix polymeric chains with the surface of clay. In order to get good dispersion/exfoliation of the silicate layers within the polymeric matrix, there should have favourable enthalpic interactions between the polymer matrix and the organically modified layered silicate surface. To evaluate the degree of interactions between PBSA and the three different kinds of surfactants used for the modification of pristine MMT, a rough estimation of solubility parameter (δ) of neat PBSA and surfactants was calculated using the group contribution method of Fedors [18]. The calculated data are presented in Table 1. The results indicate the favourable interactions between PBSA matrix and the three surfactants are in the order: 30B > 93A > 15A, in accordance with the XRD results despite the inverse order regarding the initial *d*-spacing of the organically modified clays (Table 2).

Table 2
Storage modulus, E', of neat PBSA and various nanocomposites at different temperature range

Samples	E' (GPa)			
	−60 °C	−20 °C	20 °C	60 °C
PBSA	3.6	0.72	0.53	0.3
PBSA/C15A	3.2	0.95	0.73	0.41
PBSA/C93A	4.3	1.3	0.91	0.45
PBSA/C30B	4.3	1.5	1.1	0.6

To support such results, TEM observation was used to directly and qualitatively visualize the state of silicate layers dispersion/exfoliation in the PBSA matrix. Typical TEM bright filed images of the nanocomposites are presented in Fig. 4(a–d). Fig. 4(a) is a TEM bright filed image of PBSA/CNa composite. Large agglomerates of the silicate layers are clearly seen, indicating no intercalation of PBSA chains into the silicate galleries. This is consistence with the XRD pattern observed in the case of PBSA/CNa hybrid (Fig. 3(a)). Stacked and intercalated silicate layers are clearly observed in the TEM image of PBSA/C15A nanocomposite (Fig. 4(b)), whereas coexistence of few exfoliated clay platelets and a majority of intercalated tactoids can be noticed in the case of PBSA/C93A nanocomposite (Fig. 4(c)). Highly disordered and relatively exfoliated along with very few stacked intercalated silicate layers are coexisting in the PBSA/C30B nanocomposite as can be seen in Fig. 4(d). Only the stacked intercalated silicate layers are responsible for the weak XRD reflection as was observed in Fig. 3(d), whereas the disordered or exfoliated silicate layers have no periodic stacking and thus remain XRD silent [19,20]. This type of relatively exfoliated structure with few stacked intercalated layers originates from the chemical and size inhomogeneities of the C30B layers [21,22]. Typically the large-in lateral size C30B layers create stacked intercalated structure, whereas the smaller layers tend to exfoliate. The above observations suggest that the compatibility between the surfactant modifier and the polymer matrix plays a key role for large extent of dispersion of the silicate layers within the PBSA matrix. Although C30B organoclay has the lowest interlayer spacing, it gives the highest level of dispersion/exfoliation of the silicate layers within the PBSA matrix. Such favorable interactions are attributed to interactions between 'CO' groups of the PBSA backbone (Fig. 1) and the diols species present in C30B.

3.3. Thermal properties

To elucidate the thermal behaviour of the neat PBSA and the various nanocomposites, DSC analyses were conducted and relative scans are reported in Fig. 5. Reported data were taken from a second scan to ensure reproducible thermograms free of prior thermal history effects. The glass transition temperature

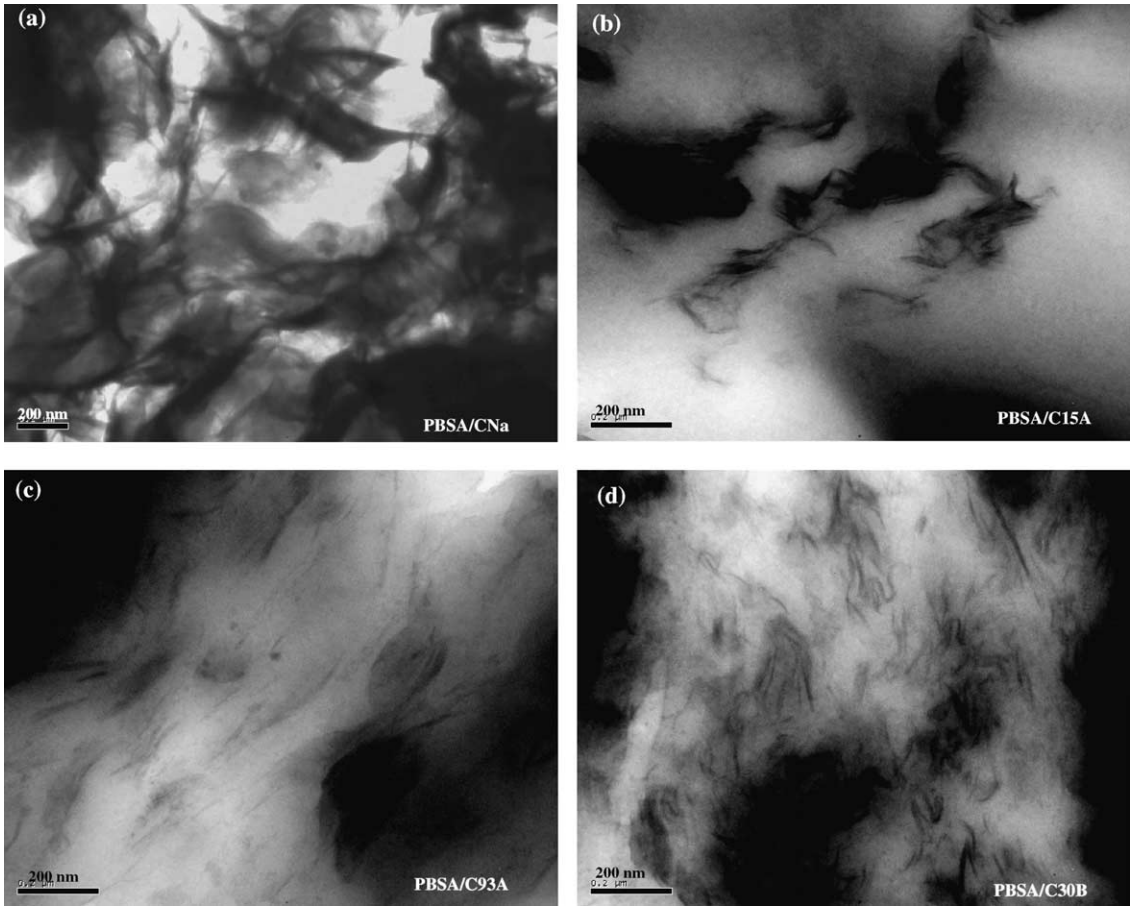

Fig. 4. TEM bright field images of (a) PBSA/CNa hybrid, (b) PBSA/C15A nanocomposite, (c) PBSA/C93A nanocomposite, and (d) PBSA/C30B nanocomposite.

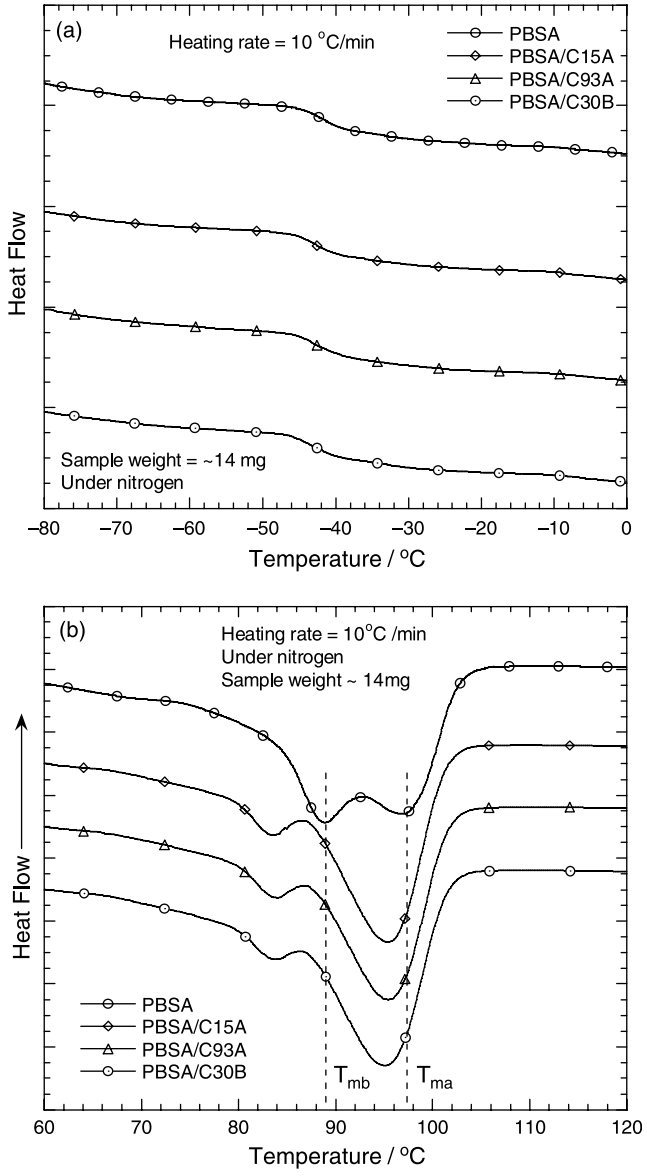

Fig. 5. DSC thermograms of neat PBSA and various nanocomposites: (a) glass transition temperature and (b) melting temperature.

(T_g) of neat PBSA and various nanocomposites are presented in Fig. 5(a). The T_g of neat PBSA systematically increases with increasing specific interactions between PBSA matrix and organic modifier used for the modification of MMT. On the other hand, all samples show two distinct melting peaks of PBSA, labelled as 'a' and 'b' (from high to low temperature), indicating two different types of crystalline lamella (Fig. 5(b)). The two melting temperatures T_{ma} and T_{mb} are of 97 and 89 °C, respectively for neat PBSA.

In the case of the nanocomposites both peak temperatures significantly shift towards lower values. This indicates that crystalline lamellar thickness of PBSA matrix has changed in the presence of silicate layers and there is a slight effect on the nature of the surfactant used for the modification of MMT. With increasing the level of specific interactions between the organic modifier and PBSA matrix, the position of the 'a' peak retains its original position but the position of 'b' peak slightly

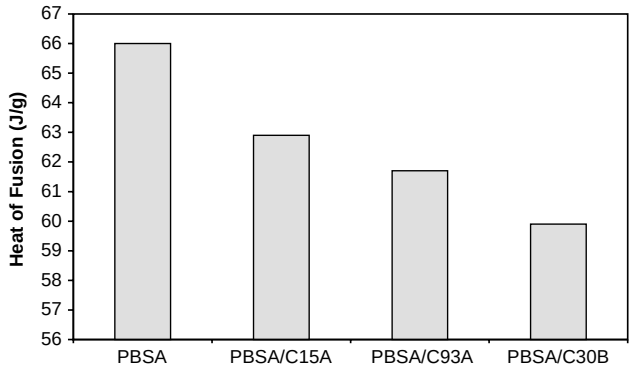

Fig. 6. Heat of fusion (ΔH J/g) (average of four independent tests with a maximum error of 2%) of neat PBSA and various nanocomposites.

moves toward higher temperatures. This suggests that the 'a' crystal developed in the presence of layered silicate particles is more perfect and it is not affected by the nature of the surfactant, and becomes less likely to undergo melting/re-crystallization [23–25]. However, organic modifiers have some effect on the melting/re-crystallization behavior of 'b' crystal.

On the other hand, the total heat of fusion (ΔH_m) of the two melting peaks of PBSA (in the case of nanocomposites ΔH_m was corrected with respect to the PBSA (per g)), calculated by integrating the area under the endothermic region of the DSC thermograms (Fig. 6), decreases systematically with increasing the degree of dispersion of the silicate layers in PBSA matrix. This decrease in crystallinity of the neat PBSA is also confirmed by the decrease in intensity (normalized with respect to the neat PBSA) of the diffraction peaks corresponding to the crystalline lamellae of PBSA as shown in Fig. 7. In the case of nanocomposites, the positions of the peaks corresponding to the crystal structure of PBSA are not altered. This means that the lattice parameters were not changed after incorporation of the silicate layers [26]. However, in the presence of C30B, the intensity of these peaks was diminished as compared to that of C93A and C15A organoclays. This is due to the high level of

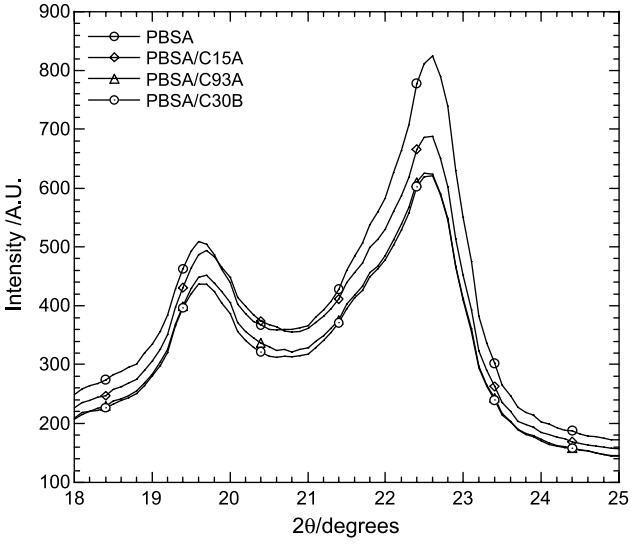

Fig. 7. XRD patterns of crystalline region of neat PBSA and various nanocomposites.

dispersion of the intercalated silicate layers in PBSA matrix, as observed in XRD patterns and TEM images (Figs. 3 and 4). Such high level of dispersion can be related to the high degree of interactions of C30B platelets with the PBSA backbone, which consequently act as obstacles for the mobility of the polymer chains to fold and join the crystallization growth front.

3.4. Dynamic mechanical analysis (DMA)

DMA has been used to examine the temperature dependence of the storage modulus (E') of PBSA upon nanocomposite formation with three different types of organoclay over the temperature range of −65 to 70 °C. Fig. 8 shows the temperature dependence of E' of the neat PBSA and the various nanocomposites. For all nanocomposites, a significant increase in E' with respect to that of the pure matrix is observed over quite all the investigated temperature range, indicating the strong effect of organoclays on the elastic properties of the neat PBSA. At low temperature, both PBSA matrix and the nanocomposites are in glassy state. An apparent glass transition (T_g) of about −42 °C was revealed by the steep decrease in E' followed by a rubbery plateau in PBSA. At around T_g of PBSA (−42 °C), the increment in E' is of about 22% for PBSA/C15A, 56% for PBSA/C93A, and 57% for PBSA/C30B, compared to that of the neat PBSA. In the temperature range between −20 and +30 °C, the three nanocomposites show significant increment in E' with respect to that of neat PBSA. For example, the magnitude of E' of PBSA/C30B is almost twice that of the pure PBSA. The level of increase in E' is again in the order of favourable interactions as discussed in the previous sections.

3.5. Tensile properties

The tensile properties of neat PBSA and the three nanocomposites are reported in Fig. 9(a)–(c) for the tensile

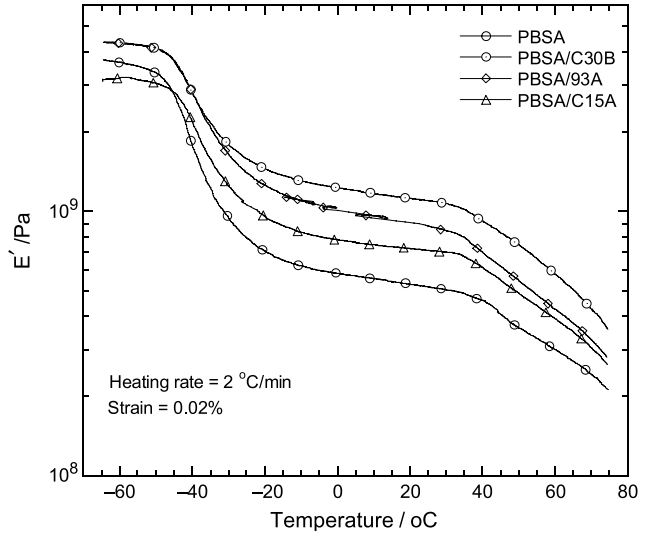

Fig. 8. Temperature dependence of storage modulus (E') of neat PBSA and various nanocomposites.

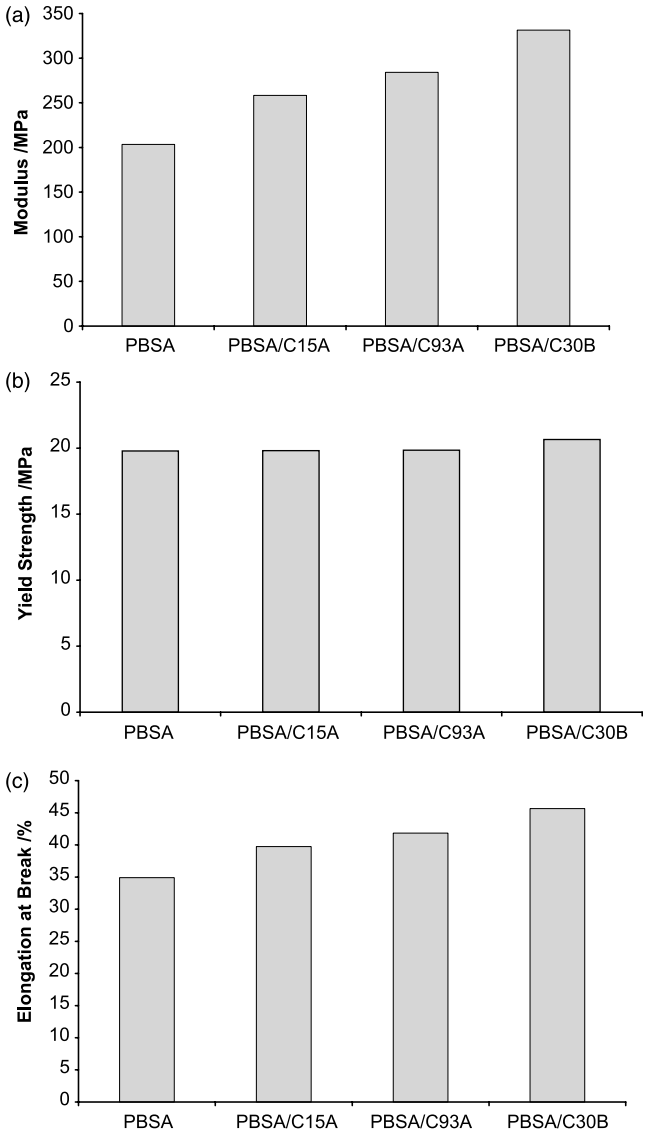

Fig. 9. Tensile properties of neat PBSA and various nanocomposites: (a) tensile Modulus, (b) tensile strength, and (c) elongation at break. Data are average of eight tests with a maximum error of 9%.

modulus, tensile yield strength, and elongation at break, respectively. The tensile modulus and elongation at break of PBSA were increased after nanocomposites formation, whereas almost no improvement in yield strength.

However, the degree of increase was found to be strongly dependent on the degree of dispersion of the silicate layers in the PBSA matrix. The increase in tensile modulus for PBSA/C15A nanocomposite is 22% compared to the neat PBSA. Such a percentage is of 33% for PBSA/C93A and 59% for PBSA/C30B. The high degree of dispersion of the intercalated silicate layers inside the PBSA matrix is the most responsible factor for this remarkable improvement in modulus in the case of PBSA/C30B nanocomposite. Because of the high degree of silicate layers dispersion, active surface area of the dispersed filler increases tremendously, which results in the higher amount of stress transfer between the matrix and the filler particles [27].

On the other hand, the tensile yield strength of PBSA was not improved after nanocomposites preparation and remains independent on the nature of the OMMT used for the nanocomposites preparation. This observation may be due to the drop in degree of crystallinity of neat PBSA after nanocomposites formation.

The elongation at break of the neat PBSA was increased after nanocomposite formation with organoclays (Fig. 9(c)). This is one of the most important property improvements in this research. Elongation at break of neat PBSA increased from 34.9 to 39.8% after nanocomposite formation with 6 wt% of C15A. As for the modulus, the elongation at break of the nanocomposites systematically increased with increasing the favourable interactions between the organic modifier and PBSA matrix. In the case of PBSA/C93A nanocomposite, the elongation at break of neat PBSA increased from 34.9 to 42%, whereas for PBSA/C30B it increased from 34.9 to 46%. Such a result is also due to the high degree of interactions between 'CO' groups on the PBSA backbone (Fig. 1) with the diols present in the C30B, which leads to the high degree of confinement of polymer chains inside the silicate layers. This situation leads to more efficient energy-dissipation mechanism in the PBSA/C30B nanocomposite and delaying the crack formation in the samples under the applied stress. Therefore, this study shows that strong matrix-filler interaction, which leads to the homogeneous dispersion of silicate layers inside the polymer matrix, is responsible for the concurrent improvement in mechanical properties in nanocomposites.

Dispersed silicate particles always have some effect on the crystallization behavior and crystallite morphology of the matrix polymer. This can influence the final mechanical properties of the nanocomposites [28,29]. However, the anisotropy and the orientation of the dispersed particles have generally a more pronounced effect on the nanocomposite mechanical properties than that of heterogeneous crystallization behaviour [30]. Although DSC measurements on the prepared nanocomposites showed some differences in the PBSA melt enthalpy, the improvement in tensile properties of PBSA/C30B nanocomposite cannot be due entirely to a change in crystallinity.

3.6. Thermal stability

Fig. 10 shows the typical TGA traces of weight loss as a function of temperature of pure PBSA and the three nanocomposites measured under air environment. It is clear from the figure that only PBSA/C30B nanocomposite shows higher thermal stability than the neat PBSA. The other OMMTs have only marginal effect of the thermal stability of the pure PBSA. The onset degradation temperature (at 3% weight loss and averages of five independent tests) as measured from the intersection of the tangent of the initial point and the inflection point) are 333.4 ± 0.7, 336.9 ± 1.9, 332.1 ± 1.5, and 328.2 ± 1.1 °C for pure PBSA, PBSA/C15A, PBSA/C93A, and PBSA/C30B nanocomposites, respectively. It is surprising to note that the onset degradation temperature of nanocomposites is inversely proportional to the degree of dispersion of silicate layers in the PBSA matrix. However, after certain percent of weight loss ($\sim 14\%$ and at 373 ± 1.8 °C), the thermal stability of nanocomposites follows the opposite trend, i.e. PBSA/C30B is more thermally stable as compared to that of PBSA/C15A, PBSA/C93A nanocomposites.

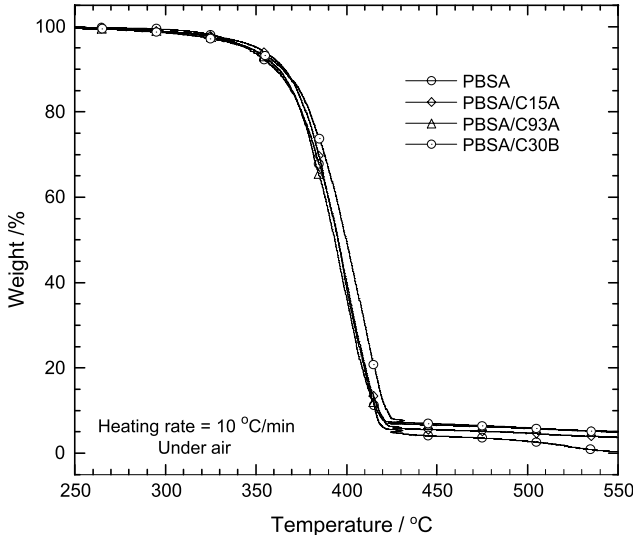

Fig. 10. Thermogravimetric analysis of neat PBSA and various nanocomposites.

The degree of dispersion of the silicate layers in PBSA matrix might be the main reason for such a behavior. The high degree of dispersion of the intercalated silicate layers enhances the performance towards thermal stability by acting as superior insulator and mass-transport barrier to the volatile products generated during thermal decomposition [31,32]. At the beginning of thermal decomposition, the stacked and intercalated silicate layers (by acting as a superior insulator compared to the exfoliated silicate layers) shift the decomposition to higher temperatures. However, after certain degree of decomposition, this heat barrier effect would result in a reverse thermal stability. In other words, the stacked and intercalated silicate layers could hold accumulated heat that could be used as a heat source to accelerate the decomposition process, in conjunction with the heat flow supplied by outside heat source. For this reason, the initial decomposition temperature of the stacked and intercalated PBSA/C15A nanocomposite is higher, but after certain temperature PBSA/C30B shows higher thermal stability although it has lower onset degradation temperature.

3.7. Melt rheology

The measurement of rheological properties of polymer nanocomposites under molten state is crucial to gain fundamental understanding of the processability and structure property relationship of these materials. Generally, the rheological behavior of polymer nanocomposite melts strongly depends on their nanostructure, their state of dispersion–distribution and their interfacial properties [33–35]. The small-amplitude oscillatory shear storage modulus, $G'(\omega)$, of the neat

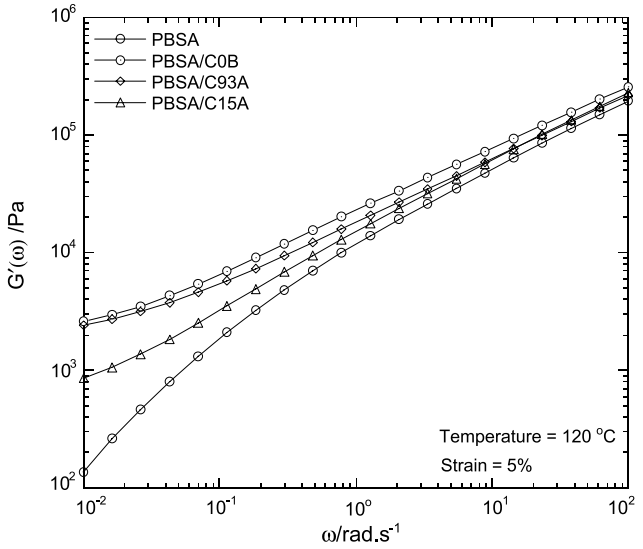

Fig. 11. Frequency dependence of dynamic storage modulus, ($G'(\omega)$), of neat PBSA and various nanocomposites.

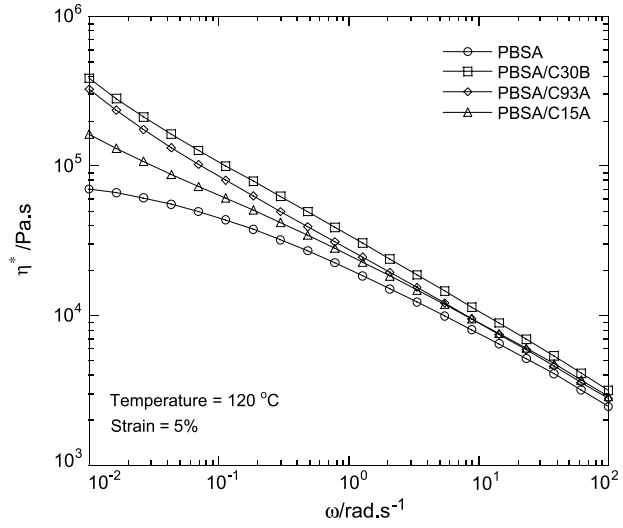

Fig. 12. Frequency dependence of dynamic complex viscosity (η^*) of neat PBSA and various nanocomposites.

PBSA and the three nanocomposites is presented in Fig. 11. As expected, $G'(\omega)$ of the nanocomposites increases with increasing the degree of dispersion of the silicate layers in the PBSA matrix over all frequency range. At high frequencies, only a slight increase in modulus with respect to that of the pure PBSA is observed. $G'(\omega)$ of the matrix and the nanocomposites decreases linearly with lowering of frequency. However, at very low frequencies a significant increase in $G'(\omega)$ is observed in the case of PBSA/C30B nanocomposite, indicating that C30B silicate layers have strong effect on the chain relaxation of PBSA. Upon increase in the favorable specific interactions between the surfactant and PBSA matrix, $G'(\omega)$ becomes a weak function of frequency and exhibits a pseudo–plateau in the terminal zone of the pure PBSA. This gradual change of behavior from liquid-like to solid-like is mainly attributed to the extent of dispersion and distribution of the clay lamellae that form three dimensional percolating networks [36,37].

This of course depends on the extent of enthalpic interactions between the PBSA backbone and the surface of OMMTs, which finally leads to the confinement of polymer chains inside the silicate galleries. Because of their highly anisotropic nature, the fully dispersed silicate layers would exhibit local correlations, which finally lead to the formation of three dimensional mesoscopic structures [37] and the tendency of formation of this mesoscopic structure gradually decreases with decreasing the degree of dispersion of intercalated silicate layers in the polymer matrix. Among the three OMMTs used for the preparation of PBSA nanocomposites, C30B has the higher degree of interactions with PBSA matrix and as a result intercalated silicate layers are relatively well dispersed in the PBSA matrix (Figs. 3 and 4). Consequently, silicate layers are highly correlated in the PBSA/C30B nanocomposite. With decreasing the degree of dispersion of intercalated layers in the PBSA matrix, the tendency of formation of this type of correlated structure is also decreased and thus the increment in modulus systematically decreases from PBSA/C30B nanocomposite to PBSA/C15A nanocomposite. The solid-like behavior can also be evidenced by the sharp increase in viscosity in the low frequency region for nanocomposites, where the pure PBSA shows rather a Newtonian behavior (Fig. 12).

The variation of the steady viscosity as a function of shear rate for the neat PBSA and the three nanocomposites is shown in Fig. 13. For comparison purposes, the small amplitude oscillatory shear viscosity is also reported on the figure. As can be expected, the steady shear viscosity and the dynamic viscosity overlap very well for the pure PBSA for $\omega = \dot{\gamma}$ (Cox–Merz rule holds). However, for the nanocomposites, such a rule fails. The steady shear viscosity becomes lower than the dynamic shear viscosity. At high shear rate, the nanocomposites loose their solid-like behavior and a rather classical Newtonian behavior is observed for the three nanocomposites.

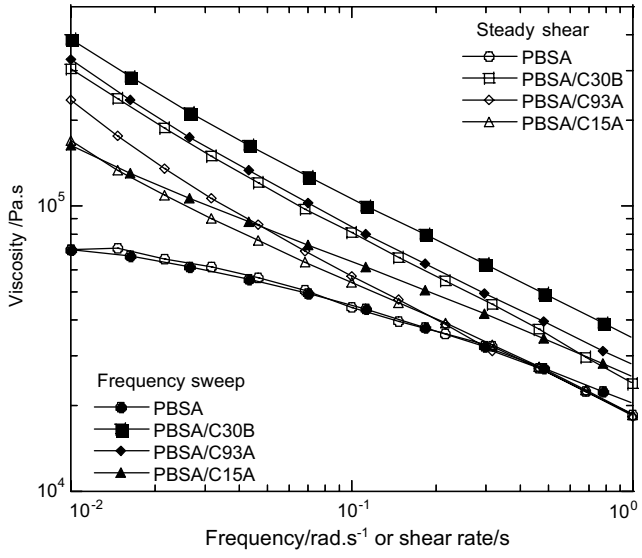

Fig. 13. Steady shear viscosity of neat PBSA and various nanocomposites as a function of shear rate.

This might be attributed to the destruction of the percolating network and the alignment of the silicate layers in the direction of flow. The polymeric chains entrapped between these thin channels of silicate layers are highly oriented and flow easily due to the loss of the density of their entanglements with the neighboring chains. This loss of local entropy decreases the local frictions and thus facilitates the chain movements in the direction of flow. Such a behavior is similar to that of layered polymer blends or reinforced polymers that show a dramatic decrease in their viscosity when submitted to a strong shear flow [38–40].

4. Conclusions

The main finding of this work is that the key parameter for high level of dispersion and distribution of the intercalated silicate layers in PBSA polymer matrix is the degree of specific interactions between the organic modifier and the matrix. By varying the polarity of the intercalants used to modify montmorillonite, a spectrum of phase-separated, intercalated and coexistence of intercalated and exfoliated morphologies were obtained. The high degree of dispersion was achieved when the solubility parameter of the modifier surfactant (C30B) was close to that of the pure PBSA. This is due to the favorable enthalpic interactions between diols present in C30B surfactant and the C=O groups present on the PBSA backbone. DSC analyses indicated that the degree of crystallinity of the neat PBSA decreased after nanocomposites formation mainly in the case of PBSA/C30B nanocomposite. The overall thermal stability of the nanocomposites was also directly related to the degree of dispersion of the silicate layers in the PBSA matrix. All nanocomposites showed significant improvement in mechanical properties.

Linear rheological material functions showed that the nanocomposites are characterized by a solid-like behavior as revealed by the presence of a low-frequency plateau on $G'(\omega)$. The magnitude of such plateau or pseudo–plateau was found to strongly depend on the level of interactions between the polymer matrix and the surfactant of the modified clay. Such specific interactions favor the state of dispersion–distribution of the clay lamellae within the polymeric matrix that lead to the formation of a long range or short range percolating network. However, such a network does not seem very stable vis-a-vis of steady shear flow. In fact steady shear flow destroys such connectivity and imparts the material with a rather Newtonian behavior in the high-shear rate region. For the moment it is not clear whether or not such percolating network can be maintained when the nanocomposites are reprocessed in machines such as extruders and injection moldings, where the flow has a complex pattern combining shear, elongational, hyperbolic and eventually chaotic flows. Such a complex relationship between flow and structure is currently under investigation.

Acknowledgements

This work was financed by the Natural Sciences and Engineering Research Council of Canada (NSERC), the Canada Research Chair on Polymer Physics and Nanomaterials, and the Steacie Fellowship grant.

References

[1] Amass W, Amass A, Tighe B. Polym Int 1998;47:89.
[2] Okada M. Prog Polym Sci 2002;27:87.
[3] Tokiwa Y, Calabia BP. Biotech Lett 2004;26:1181.
[4] Hoshino A, Isono Y. Biodegradation 2002;13:141.
[5] Leayersuch R, Biodegradable polyesters: packaging goes green, Plastic Technology Online Article; 09/05/02.
[6] Sinha Ray S, Bousmina M. Prog Mater Sci 2005;50:962.
[7] Sinha Ray S, Okamoto M. Prog Polym Sci 2003;28:1539.
[8] Sinha Ray S, Biswas M. Adv Polym Sci 2001;55:167.
[9] Alexander M, Dubois Ph. Mater Sci Eng 2000;R28:1.
[10] LeBaron PC, Wang Z, Pinnavaia TJ. Appl Clay Sci 1999;15:11.
[11] Giannelis EP. Adv Mater 1996;8:29.
[12] Grim RE. Clay mineralogy. New York: McGraw-Hill; 1953.
[13] Aranda P, Ruiz-Hitzky E. Chem Mater 1992;4:1395.
[14] Greeland DJ. J Colloid Sci 1963;18:647.
[15] Lepoittevin B, Devalckenaere M, Pantoustier N, Alexandre M, Calberg C, Jerome R, et al. J Mater Chem 2002;12:3528.
[16] Viville P, Lazzaroni R, Pollet E, Alexandre M, Dubois P. J Am Chem Soc 2004;126:9007.
[17] Sinha Ray S, Bousmina M. Macromol Rapid Commun 2005;26:1639.
[18] Krevelen DWV. Properties of polymers. Amsterdam, The Netherlands: Elsevier; 1990.
[19] Sinha Ray S, Yamada K, Okamoto M, Fujimoto Y, Ogami A, Ueda K. Polymer 2003;44:6633.
[20] Dritis VA. X-ray diffraction by disordered lamellar structures. New York: Springer; 1990 p. 21.
[21] Sinha Ray S, Yamada K, Okamoto M, Ogami A, Ueda K. Macromol Rapid Commun 2002;23:943.
[22] Sinha Ray S, Yamada K, Okamoto M, Ogami A, Ueda K. Chem Mater 2003;15:1456.
[23] Ghosh AK, Woo EM. J Mater Chem 2004;14:3034.
[24] Ghosh AK, Woo EM. Polymer 2004;45:4749.
[25] Priya L, Jog JP. J Polym Sci, Part B: Polym Phys 2002;40:1682.
[26] Sinha Ray S, Bousmina M, Okamoto K. Macromol Mater Eng 2005;290:759.
[27] Mishra JK, Hwang KJ, Ha CS. Polymer 2005;46:1995.
[28] Nam YJ, Sinha Ray S, Okamoto M. Macromolecules 2003;36:7126.
[29] Maiti P, Nam PH, Okamoto M, Usuki A, Hasegawa N. Macromolecules 2002;35:2042.
[30] Osman MA, Rupp Jörg EP, Suter UW. Polymer 2005;46:1653.
[31] Gilman JW, Jackson CL, Morgan AB, Harris R. Chem Mater 2000;12:1866.
[32] Lim ST, Hyun YH, Choi HJ, Jhon MS. Chem Mater 2002;14:1839.
[33] Sinha Ray S, Okamoto K, Okamoto M. Macromolecules 2003;36:2355.
[34] Sinha Ray S, Maiti P, Okamoto M, Yamada K, Ueda K. Macromolecules 2002;25:3104.
[35] Krishnamoorti R, Koray Y. Curr Opin Colloid Interface Sci 2001;6:464.
[36] Bousmina M, Muller R. J Rheol 1993;37:663.
[37] Ren J, Silva AS, Krishnamoorti R. Macromolecules 2000;33:3739.
[38] Bousmina M, Muller R. Rheol Acta 1996;35:369.
[39] Bardollet P, Bousmina M, Muller R. Polym Adv Technol 1995;6:301.
[40] Bousmina M, Palierne JF, Utracki LA. Polym Eng Sci 1999;39:1049.